

Shahila Mehboob,* Kent Truong,
Bernard D. Santarsiero and
Michael E. Johnson*

Center for Pharmaceutical Biotechnology,
University of Illinois at Chicago, 900 South
Ashland Avenue, Chicago, IL 60607, USA

Correspondence e-mail: shahila@uic.edu,
mjohnson@uic.edu

Received 4 August 2010
Accepted 6 October 2010

PDB Reference: enoyl-acyl carrier protein
reductase, 3nrc.

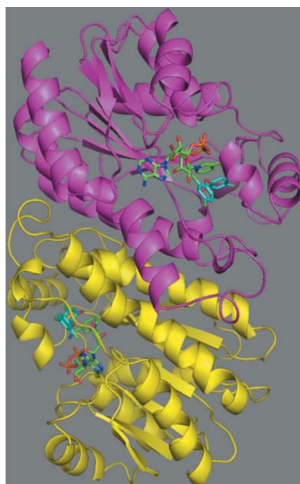
Structure of the *Francisella tularensis* enoyl-acyl carrier protein reductase (FabI) in complex with NAD⁺ and triclosan

Enoyl-acyl carrier protein reductase (FabI) catalyzes the last rate-limiting step in the elongation cycle of the fatty-acid biosynthesis pathway and has been validated as a potential antimicrobial drug target in *Francisella tularensis*. The development of new antibiotic therapies is important both to combat potential drug-resistant bioweapons and to address the broader societal problem of increasing antibiotic resistance among many pathogenic bacteria. The crystal structure of FabI from *F. tularensis* (FtuFabI) in complex with the inhibitor triclosan and the cofactor NAD⁺ has been solved to a resolution of 2.1 Å. Triclosan is known to effectively inhibit FabI from different organisms. Precise characterization of the mode of triclosan binding is required to develop highly specific inhibitors. Comparison of our structure with the previously determined FtuFabI structure (PDB code 2jyy) which is bound to only NAD⁺ reveals the conformation of the substrate-binding loop, electron density for which was missing in the earlier structure, and demonstrates a shift in the conformation of the NAD⁺ cofactor. This shift in the position of the phosphate groups allows more room in the active site for substrate or inhibitor to bind and be better accommodated. This information will be crucial for virtual screening studies to identify novel scaffolds for development into new active inhibitors.

1. Introduction

Francisella tularensis is a highly virulent and contagious Gram-negative bacterium that is the causative agent of the disease tularemia. This intracellular bacterium primarily infects macrophages and evades the immune system. If the bacteria are inhaled, symptoms of the disease include an abrupt onset of fever, chills, headache, muscle aches, joint pain and progressive weakness. Tularemia can be fatal if the person is not treated with appropriate antibiotics. The Centers for Disease Control and Prevention regard *F. tularensis* as a viable bioweapon agent and have classified it as a Category A agent. Currently, streptomycin and gentamicin are used to treat tularemia; however, neither are orally administered (Lu & Tonge, 2008). Doxycycline and ciprofloxacin are also used to treat the disease and are orally administered, but are not ideal for the treatment of tularemia. Thus, there is a clear and urgent need for the development of novel therapeutics.

The type I fatty-acid synthesis (FAS I) pathway found in mammals takes place on a large single multifunctional protein in which active sites catalyzing different steps are found in different domains. Bacterial type II fatty-acid synthesis (FAS II), on the other hand, is carried out by a series of discrete enzymes, unlike the mammalian counterpart. The NADH-dependent enoyl reductase (FabI) catalyzes the final rate-limiting step in the elongation cycle and is an important component of the FAS II system (Bergler *et al.*, 1996). The FabI enzymes are members of the short-chain alcohol dehydrogenase/reductase superfamily characterized by a catalytic triad that includes two tyrosines and a lysine residue (Parikh *et al.*, 1999; Wen *et al.*, 2009). While the overall structural homology between FabIs from different organisms is high, variability exists in a mobile loop of amino acids that covers the active site (the substrate-binding loop).



No electron density is seen for this loop when substrate or inhibitor is not bound in the active site (Baldock *et al.*, 1996; Priyadarshi *et al.*, 2010). However, an α -helical conformation is observed when substrate or inhibitor is bound in the active site (Baldock *et al.*, 1996; Levy *et al.*, 1999; Stewart *et al.*, 1999).

We have determined the crystal structure of FabI from *F. tularensis* (FtuFabI) bound to NAD⁺ and triclosan at a resolution of 2.1 Å. Triclosan [5-chloro-2-(2,4-dichlorophenoxy)phenol] is a broad-spectrum antifungal and antimicrobial agent and effectively inhibits the FabI enzyme from numerous bacteria. While the broad specificity of triclosan has already been exploited by incorporating it into a number of widely used consumer products, triclosan can also provide a basis for designing highly organism-specific inhibitors. Knowledge of the precise nature of the interactions between triclosan and FabI from *F. tularensis* is required to improve the specificity and efficacy of newly designed inhibitors. This newly determined structure also provides a more accurate model for virtual screening.

2. Materials and methods

2.1. Protein preparation

The gene for FabI (from *F. tularensis* subsp. *tularensis* Schu4) was commercially synthesized (Bio Basic Inc., Canada) after codon optimization. The gene was ligated into a pET-15b vector with an N-terminal His tag and transformed into *Escherichia coli* BL21 (DE3) cells. The cells were grown at 310 K and induced with 1 mM IPTG when the OD reached 0.5. The cells were harvested after an additional 4 h of growth. Sonication was used to lyse the cells and the supernatant was loaded onto a nickel-chelated His-Trap column (GE Healthcare) and eluted with a stepwise gradient of imidazole in 50 mM Tris, 500 mM NaCl pH 8.0. The final purification step used a size-exclusion column (Superdex-200 26/60 from GE Healthcare) previously equilibrated with buffer consisting of 50 mM Tris, 100 mM

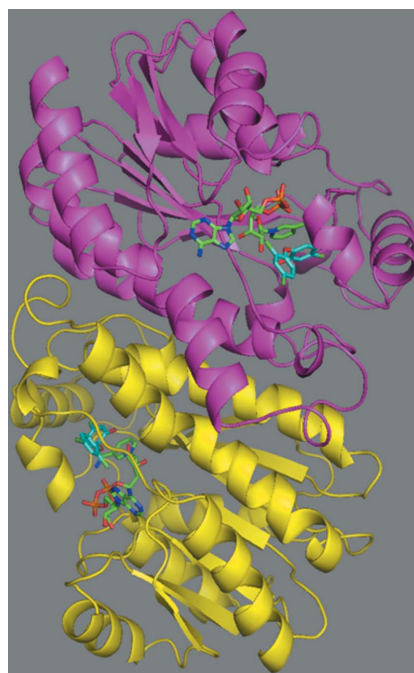


Figure 1
Crystal structure of FtuFabI in complex with NAD⁺ and triclosan. The two chains in the asymmetric unit are colored magenta and yellow. The active site is indicated by the presence of NAD⁺ (green backbone) and triclosan (cyan backbone).

Table 1
Data-collection and refinement statistics.

Data collection	
Space group	<i>P</i> 2 ₁ 2 (No. 18)
Unit-cell parameters (Å)	<i>a</i> = 123.08, <i>b</i> = 85.12, <i>c</i> = 51.76
Resolution (Å)	2.0
No. of reflections	345331
No. of averaged reflections (unique reflections)	36922
<i>R</i> _{merge} (%)	15.0
<i>I</i> / <i>σ</i> (<i>I</i>)	16.0
Completeness (%)	85.8
Refinement	
Resolution range (Å)	20.0–2.1
No. of reflections	30957
No. of reflections in test set	1560
Completeness (%)	95.3
<i>R</i> _{cryst} (%)	18.6
<i>R</i> _{free} (%)	24.2
Wilson <i>B</i> factor (Å ²)	38.9
Average <i>B</i> factor (protein) (Å ²)	33.9
No. of protein molecules in asymmetric unit	2
R.m.s.d.s from ideal geometry	
Bond lengths (Å)	0.006
Bond angles (°)	1.024
Ramachandran plot	
Allowed (%)	96.5
Generously allowed (%)	0.2
Disallowed (%)	0.00

NaCl pH 8.0 with 1 mM DTT. The FabI enzyme was soluble when overexpressed and was purified to >98% purity.

2.2. Crystallization and X-ray data collection

The FabI stock solution was concentrated to 17 mg ml⁻¹ in 50 mM Tris, 100 mM NaCl pH 8.0 and was then mixed with 5 mM NAD⁺ and 0.5 mM triclosan. Crystallization experiments were performed by the sitting-drop vapor-diffusion method using commercially available screens. 400 nl protein solution was mixed with 400 nl reservoir solution and the plates were incubated at 289 K. Crystals appeared in 4 d in one of the conditions from Wizard Screen II consisting of 2 M ammonium sulfate, 0.1 M phosphate–citrate buffer pH 4.2. Crystals were cryoprotected by soaking them in a solution containing 10% glycerol in mother liquor. Data were collected from one crystal on the SER-CAT 22-BM beamline at the Advanced Photon Source, Argonne National Laboratory using a wavelength of 1 Å, a sample-to-detector distance of 220 mm and an oscillation angle of 0.5°. A complete data set was recorded on a MAR CCD 225 to a resolution of 2.0 Å. Diffraction data were processed and scaled using *XDS* (Kabsch, 2010). The crystal belonged to space group *P*2₁2₁2 and contained two monomers in the asymmetric unit, with a solvent content of 45%. The unit cell-parameters and data-collection statistics are given in Table 1.

2.3. Structure solution and refinement

The structure of FtuFabI (complexed with NAD⁺ and triclosan) was solved by molecular replacement using *Phaser* (McCoy *et al.*, 2007) in the *CCP4* program suite (Collaborative Computational Project, Number 4, 1994) with the coordinates of a single chain of FtuFabI complexed with NAD⁺ (PDB code 2jji; Lu *et al.*, 2009) as a model. Refinement was carried out using *REFMAC5.5* (Vagin *et al.*, 2004). Refinement included data in the resolution range 20–2.1 Å. A total of 5% of the data were kept aside for *R*_{free} calculations. The model was built using the program *Coot* (Emsley *et al.*, 2010). After a few cycles of restrained refinement, significant electron density was observed in the active site and the atoms of NAD⁺ and triclosan were placed. Water molecules were added using *PHENIX* (Adams *et al.*, 2010), followed by final refinement with *PHENIX*. The final refine-

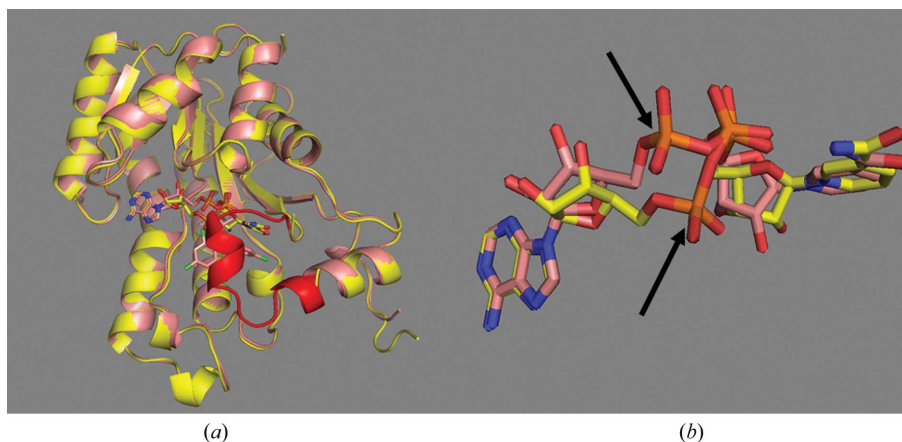


Figure 2
 (a) Overlap of FtufabI in complex with NAD⁺ (PDB code 2jyy; yellow) onto FtufabI in complex with NAD⁺ and triclosan (salmon). The substrate-binding loop for which no electron density is seen in 2jyy is colored red. The active-site location is indicated by the NAD⁺ and triclosan shown as stick models. The substrate-binding loop (red) sits over the active site, forming a lid. (b) Overlap of the orientation of NAD⁺ in the active site of our structure (C atoms in salmon pink) and in the 2jyy structure (C atoms in yellow). The shift in the backbone phosphate is indicated by the arrows.

ment statistics together with the statistics concerning the geometry of the final models are given in Table 1. The final model has an R_{cryst} of 18.6%, an R_{free} of 24.3% and a map figure of merit (FOM) of 0.80. The model was validated using *MolProbity* (Chen *et al.*, 2010) and *PROCHECK* (Laskowski *et al.*, 1993). The majority of the residues lie in the most favored regions of the Ramachandran plot and the remaining residues are in the generously allowed regions. The coordinates of the structure of FtufabI complexed with NAD⁺ and triclosan have been deposited in the PDB with accession code 3nrc.

3. Results and discussion

3.1. Structure of FtufabI

FtufabI was purified using His-tag affinity chromatography followed by size-exclusion chromatography, providing pure protein (>98%). The enzyme consists of 280 amino acids, including a 20-residue His tag, and has a molecular weight of 29 968 Da. The asymmetric unit in the crystal structure of FtufabI contains two monomers with an average root-mean-square difference (r.m.s.d.) between them of 0.19 Å (all-atom alignment), indicating that they have nearly identical structures (Fig. 1). The interface area between the two chains is 1660 Å² (calculated using *PDBSum*). Using dynamic light-scattering studies and size-exclusion studies, we have found that FtufabI exists in different oligomeric forms that are dependent on concentration. At concentrations from 60 to 138 μM FtufabI exists as a tetramer, while at concentrations below 8 μM a dimeric unit is seen (Table 2). Between 40 and 14 μM we see either a dimer–tetramer equilibrium or trimeric units. The experiment is unable to distinguish between these possibilities. We assayed the activity of FabI by following the fluorescence change of NADH as it is converted to NAD⁺. In these assays the concentration of FtufabI used was 0.1 μM. At these concentrations we believe that the enzyme may be dimeric or even monomeric. However, this does not seem to affect the activity of the enzyme. Our data clearly indicate that FtufabI exists as a tetramer above concentrations of 60 μM, as in the crystallization experiments, in which a 500 μM solution of FtufabI was used. As the asymmetric unit in the crystal structure contains two chains, the tetramer can be generated by the operation $x, -1 - y, -z$. The buried surface area between the two dimers in the tetramer is 1312 Å² (between each chain), which is significant enough to lead us to conclude that the crystal contains tetramers. Our structure of FtufabI

is similar to those of FabI from other organisms (*E. coli*, *Mycobacterium tuberculosis*, *Bacillus anthracis*, *Helicobacter pylori* and *Staphylococcus aureus*, among others), including a previously determined structure from *F. tularensis* which is a complex of FabI with NAD⁺ (PDB code 2jyy). Superposition of one chain of the triclosan-bound FtufabI with one chain of the previously determined NAD⁺ complex of FtufabI results in an r.m.s. difference of 0.35 Å (all-atom alignment), indicating that the overall structure of FtufabI does not change upon binding triclosan. However, the substrate-binding loop (residues 191–205) undergoes a major conformational change upon binding to triclosan and forms a lid on top of the triclosan moiety and the nicotinamide group that shields them from the solvent (Fig. 2a). The residues in this loop are not observed in the 2jyy structure as no density for the loop was seen in this structure. This implies that this region is either very flexible in the apo form or is disordered prior to binding the substrate or inhibitor. Additionally, we find that the backbone phosphate groups of the NAD⁺ in our structure adopt a different conformation to that found in the 2jyy structure (Fig. 2b). It

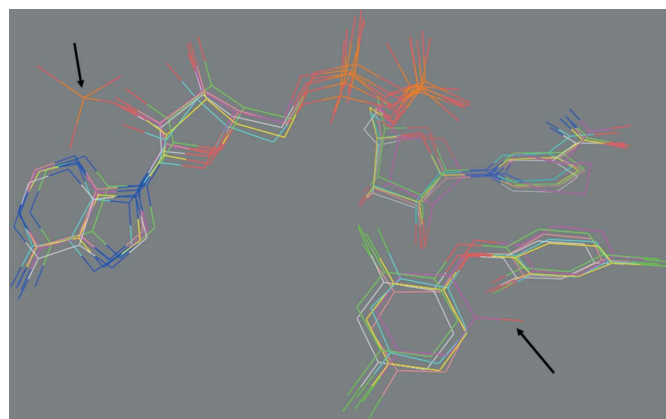


Figure 3
 Overlap of NAD⁺ and triclosan from known FabI structures. The orientation of NAD⁺ and triclosan in our structure (C atoms in green) is similar to the orientations of NAD⁺ in *B. anthracis* (C atoms in yellow), *E. coli* (C atoms in salmon), *H. pylori* (C atoms in white), *M. tuberculosis* (C atoms in cyan) and NADP⁺ in *S. aureus* (C atoms in magenta) FabI. The orientation of triclosan is also similar to that in other structures except for the orientation of triclosan in *S. aureus*, in which the OH group is in a different orientation. The arrows indicate the *S. aureus* NADP⁺ and triclosan.

is possible that since the substrate-binding loop in 2jyy is disordered (or flexible) NAD⁺ is not in a single conformation. This shift in the backbone phosphate of NAD⁺ better accommodates triclosan in the active site. We have compared known NAD⁺ and triclosan conformations in FabIs from different organisms and find that the overall conformations of NAD⁺ and triclosan are similar to our structure, except for the case of *S. aureus* FabI, in which the orientation of triclosan is substantially different (Fig. 3).

FabI is a member of the short-chain alcohol dehydrogenase/reductase family. This superfamily is characterized by a conserved triad of active-site residues. In FtufabI the triad is comprised of Tyr146, Tyr156 and Lys163. Triclosan is stabilized in the active site by

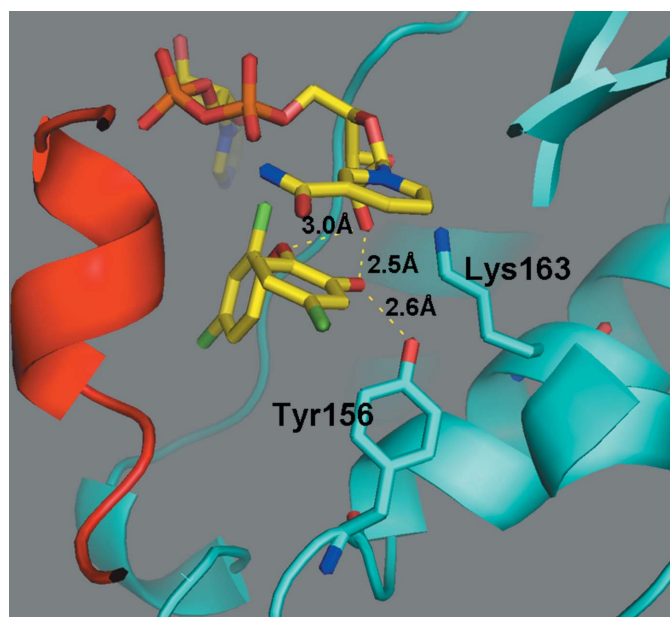


Figure 4

Close-up side view of the active site of FtufabI. Triclosan forms three hydrogen bonds: two with NAD⁺ and one with Tyr156. Lys163 also forms a hydrogen bond with NAD⁺ (not shown). The substrate-binding loop (in red) is hydrophobic and packs against triclosan, forming a compact enclosure.

Table 2

Dynamic light-scattering and size-exclusion data.

Concentration (μM)	Concentration (mg ml^{-1})	Molecular weight (kDa)	No. of monomeric units
Dynamic light-scattering data			
138	4.1	128	4.2
100	3.0	124	4.1
80	2.4	120	4.0
60	1.8	120	4.0
40	1.2	108	3.6
20	0.6	102	3.4
14	0.4	100	3.3
5	0.15	60	2.0
Size-exclusion data			
8	0.23	55	1.8
2	0.06	54	1.8
1.8	0.055	54	1.8
0.5	0.01	56	1.9

hydrophobic interactions and through three hydrogen bonds, one to the OH of Tyr156 and two to O2D of NAD⁺ (Fig. 4). The π - π stacking interactions between the A ring of triclosan and the nicotinamide ring are conserved in the known ternary complexes. No hydrogen bonding is seen between the triclosan and the substrate-binding loop. Triclosan sits in a hydrophobic pocket created by the substrate-binding loop and other residues in the active site. We suggest that the hydrophobic nature of triclosan causes the substrate-binding loop to position itself over the active site and become more ordered or rigid.

Analysis of structures of FabI from other organisms reveal that in the apo form regions of FabI are either partially disordered or very flexible as no density is seen for a number of residues in the crystal structure, as seen, for example, in FabI from *S. aureus* (PDB code 3gns; Priyadarshi *et al.*, 2010). Upon comparison with the crystal structure of *E. coli* bound to NAD⁺ (PDB code 1dfi; Baldock *et al.*, 1996) we see that once NADH binds in the active site the region lining the entrance to the active site becomes structured (Figs. 5*a* and 5*b*), similar to that seen in the case of the 2jyy structure. When the substrate or inhibitor (triclosan in this case) binds in the active site over NADH, the substrate-binding loop then becomes ordered (or structured) and forms a lid over the active site, resulting in a compact enclosure that allows catalysis to take place (Fig. 5*c*).

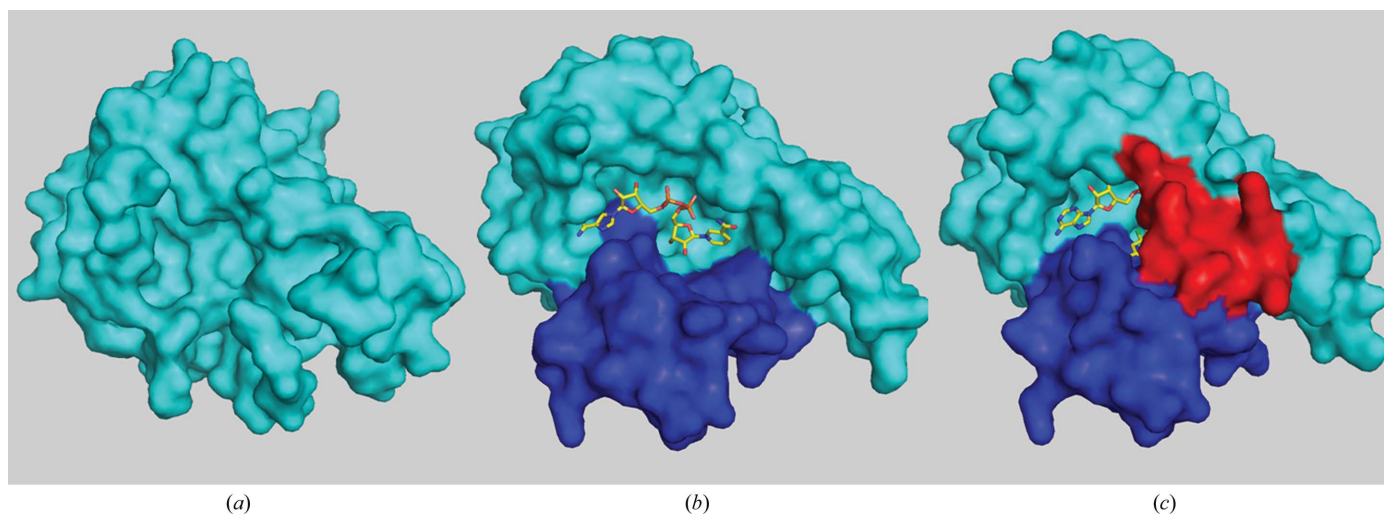


Figure 5

Comparison of the structures of apo FabI, FabI bound to NAD⁺ and FabI bound to NAD⁺ and triclosan. (*a*) Apo FabI from *S. aureus* (PDB code 3gns). (*b*) FabI from *E. coli* bound to NAD⁺ (PDB code 1dfi). Electron density for the region lining the entrance to the active site is absent in the apo form, but when NAD⁺ is bound in the active site electron density for this region is visible, revealing a structured region. This region is colored blue. (*c*) FabI from *F. tularensis* bound to both NAD⁺ and triclosan. The substrate-binding loop (red) for which density was not seen in the previous structures is now visible and is structured, clearly forming a lid over the active site

4. Conclusions

We have determined the crystal structure of *F. tularensis* FabI in complex with NAD⁺ and the inhibitor triclosan. Our structure provides a clearly visible substrate-binding loop; no density was seen for this loop in the previously determined FtufabI structure in complex with NAD⁺ only (PDB code 2jyy). Additionally, in our model the orientation of the NAD⁺ differs from that in 2jyy. This finding significantly enhances our work which, together with a better model (2.1 Å resolution compared with the previous structure at 2.9 Å), provides a more accurate model that can now be used for computational screening purposes.

We thank Drs Rory Mulligan and Andrzej Joachimiak for assistance with and use of the crystallization robotics equipment at the Structural Biology Center, Argonne National Laboratory. This work was supported by National Institutes of Health Grant U01AI077949. Data were collected on the Southeast Regional Collaborative Access Team (SER-CAT) 22-BM beamline at the Advanced Photon Source, Argonne National Laboratory. Use of the Advanced Photon Source was supported by the US Department of Energy, Office of Science, Office of Basic Energy Sciences under Contract No. W-31-109-Eng-38. We also thank Dr Karl Volz for assistance and use of his Dynamic Light Scattering Instrument.

References

Adams, P. D. *et al.* (2010). *Acta Cryst.* **D66**, 213–221.

- Baldock, C., Rafferty, J. B., Sedelnikova, S. E., Baker, P. J., Stuitje, A. R., Slabas, A. R., Hawkes, T. R. & Rice, D. W. (1996). *Science*, **274**, 2107–2110.
- Bergler, H., Fuchsichler, S., Hogenauer, G. & Turnowsky, F. (1996). *Eur. J. Biochem.* **242**, 689–694.
- Chen, V. B., Arendall, W. B., Headd, J. J., Keedy, D. A., Immormino, R. M., Kapral, G. J., Murray, L. W., Richardson, J. S. & Richardson, D. C. (2010). *Acta Cryst.* **D66**, 12–21.
- Collaborative Computational Project, Number 4 (1994). *Acta Cryst.* **D50**, 760–763.
- Emsley, P., Lohkamp, B., Scott, W. G. & Cowtan, K. (2010). *Acta Cryst.* **D66**, 486–501.
- Kabsch, W. (2010). *Acta Cryst.* **D66**, 125–132.
- Laskowski, R. A., MacArthur, M. W., Moss, D. S. & Thornton, J. M. (1993). *J. Appl. Cryst.* **26**, 283–291.
- Levy, C. W., Roujeinikova, A., Sedelnikova, S., Baker, P. J., Stuitje, A. R., Slabas, A. R., Rice, D. W. & Rafferty, J. B. (1999). *Nature (London)*, **398**, 383–384.
- Lu, H., England, K., Am Ende, C., Truglio, J. J., Luckner, S., Reddy, B. G., Marlenee, N. L., Knudson, S. E., Knudson, D. L., Bowen, R. A., Kisker, C., Slayden, R. A. & Tonge, P. J. (2009). *ACS Chem. Biol.* **4**, 221–231.
- Lu, H. & Tonge, P. J. (2008). *Acc. Chem. Res.* **41**, 11–20.
- McCoy, A. J., Grosse-Kunstleve, R. W., Adams, P. D., Winn, M. D., Storoni, L. C. & Read, R. J. (2007). *J. Appl. Cryst.* **40**, 658–674.
- Parikh, S., Moynihan, D. P., Xiao, G. & Tonge, P. J. (1999). *Biochemistry*, **38**, 13623–13634.
- Priyadarshi, A., Kim, E. E. & Hwang, K. Y. (2010). *Proteins*, **78**, 480–486.
- Stewart, M. J., Parikh, S., Xiao, G., Tonge, P. J. & Kisker, C. (1999). *J. Mol. Biol.* **290**, 859–865.
- Vagin, A. A., Steiner, R. A., Lebedev, A. A., Potterton, L., McNicholas, S., Long, F. & Murshudov, G. N. (2004). *Acta Cryst.* **D60**, 2184–2195.
- Wen, L., Chmielowski, J. N., Bohn, K. C., Huang, J.-K., Timsina, Y. N., Kodali, P. & Pathak, A. K. (2009). *Protein Expr. Purif.* **65**, 83–91.